Appendix

Contents

Appendix 1. Complementary details on the methodology

Samples from participants

In total, 87 patients with chronic obstructive pulmonary disease (COPD) and controls were included in the study.

For the main study, which included patients with Global Initiative for Chronic Obstructive Lung Disease (GOLD) Stage I–III COPD and controls (N=57), surgical tissues were collected at Skåne University Hospital in Lund, Sweden, and processed for histologic analysis, as previously described [E1, E2]. The severity of COPD spanned from mild to very severe (GOLD I–IV). Lung resection samples were obtained from patients with mild to severe (GOLD I–III) COPD, as well as never-smokers and smoking controls, who were undergoing surgery for well-delineated tumours. Only patients with solid, well-defined tumours were included, and the present tissue samples were obtained as far from the tumour as possible. Explanted lung tissue from lung transplantation surgery was obtained from patients with very severe (GOLD Stage IV) COPD. For all groups, multiple lung tissue slices (approximately 15-mm thick) were immediately immersed in standard 4% buffered paraformaldehyde fixative after surgery. After fixation for approximately 24 hours, the tissues were trimmed into blocks, dehydrated, and embedded into paraffin blocks containing multiple anatomic regions of the lungs (alveolar parenchyma, bronchioles and pulmonary vessels). Separate large airway blocks (i.e., bronchi) were obtained from the explanted lungs (GOLD IV COPD patients) only. Importantly, the tissue preparation procedures were the same for all patient groups.

Inclusion criteria for the patients with COPD were a significant history of tobacco smoking and spirometrically defined COPD diagnosis according to GOLD guidelines. Thus, all included patients had a persistent airflow obstruction (forced expiratory volume in 1 second/forced vital capacity <0.7). Exclusion criteria were any atopy or allergic disease as well as any non-COPD airway-related disease (including any physician-diagnosed asthma and upper airway conditions such as rhinitis or nasal polyposis). Smoker or never-smoker control patients had no history of respiratory disease and no symptoms of infections for at least 4 weeks prior to surgery.

In additional to the surgical samples, bronchial biopsies were collected from 30 separate patients with COPD (GOLD I–II; n=13) and smoker and never-smoker controls (n=17) to increase the number of bronchial samples and available samples with appropriate messenger ribonucleic acid (mRNA)–preserved tissues for *in-situ* hybridisation (ISH). These patient groups and clinical characteristics are presented in Table E2. Bronchoscopy was performed after local anaesthesia with a flexible bronchoscope (Olympus IT160, Tokyo, Japan). Before bronchoscopy, the patients received oral midazolam (1 mg/10 kg) and intravenous (IV) Glykopyrron (0.4 mg). Local anaesthesia was given as Xylocain spray: local and through-spray catheter. Just before the procedure, alfentanyl (0.1–0.2 mg/10 kg) was given intravenously and extra intravenous midazolam was given when needed. Central airway biopsies were taken from the segmental or subsegmental carina in the lower and upper right lobe. Oxygen was given as needed during and after the procedure.

All clinical procedures were performed at the Department of Thoracic Surgery or Department Respiratory Medicine and Allergology, Lund/Skåne University Hospital, Sweden, and all

procedures were approved by the local Swedish Research Ethics Committee in Lund, Sweden. All patients signed informed consent to participate.

Immunohistochemistry

After antigen retrieval in a PT Link machine (Dako, Glostrup, Denmark), tissue sections were subjected to double and triple immunostaining using an automated immunohistochemistry robot (Autostainer Plus, Dako), as previously described [E1, E2]. For the main analysis, a triple immunohistochemistry (IHC) protocol was used to simultaneously detect eosinophils, basophils, and the Th_2 surrogate marker, GATA3 [E3, E4].

Each slide was incubated in dual endogenous enzyme-blocking reagent for 10 minutes to suppress endogenous alkaline phosphatase and peroxidase in paraffin-embedded tissue sections. The section was incubated for 1 hour in diluted antibodies against GATA3, followed by incubation for 30 minutes with polymer horseradish peroxidase (HRP)-linked secondary antibodies (EnVision™ G|2 Doublestain System Rabbit/Mouse, K5361, Dako). GATA3 cells were visualised using diaminobenzidine (DAB) (brown-coloured product, 3,3' DAB, K3468, Dako). Slides were rinsed with buffer after each step, and they were rinsed with distilled water after tissue sections were subjected to a chromogen.

Next, the sections were subjected to multiple staining with denaturing solution (DNS001H, L, Biocare Medical, Concord, CA, USA) for 5 minutes. This step was performed to denature residual antibodies to avoid cross reactivity. Tissue sections were further incubated with primary antibodies against eosinophil cationic protein (ECP) for 1 hour, followed by incubation for 30 minutes with polymer HRP-linked secondary antibodies (EnVision™ Peroxidase/DAB Detection System Kit, Rabbit/Mouse, K5007, Dako). Green-coloured

eosinophils were detected using Vina Green™ (Biocare Medical) as chromogen for this enzyme. This was followed by a 5-minute blocking and denaturing step, as previously mentioned.

For the last step, tissue sections were incubated for 1 hour in diluted BB1 antibodies followed by incubation for 1 hour with anti-mouse polymer alkaline phosphatase (EnVision G|2 Doublestain System Rabbit/Mouse, K5361, Dako). These basophils were visualised using the Liquid Permanent Red Substrate Kit (K0640, Dako). Slides were then rinsed in distilled water, counterstained with Mayer's hematoxylin solution (Sigma-Aldrich, Saint Louis, MO, USA), and mounted with Pertex® (Mitsui & Co., Ltd., Toyko, Japan).

Th_2 lymphocytes were immune-stained and identified as $GATA3^+$, $CD4^+$ cells. Type 2 innate lymphoid cells were identified as lineage-negative, $CD25^+$, $GATA3^+$ cells, as recently described [E5]. The proportion and relative abundance of Th2 vs. ILC2 cells were quantified in eosinophil-high COPD patients and expressed as percentage (%) ILC2 (and Th2 cells) of the total sum of ILC2 and Th2 cells.

Several standard IHC cell markers were also used for general immune cell exploration and to identify chemokine-expressing cells. All antibodies used have been extensively validated for use in clinical diagnosis or research and are listed in Supplemental Table E1.

In-Situ **Hybridization**

Human and mouse eotaxin-1 (CCL11) and eotaxin-2 (CCL24) mRNA were visualised using the RNAscope 2.5 formalin-fixed paraffin-embedded assay kit (Advanced Cell Diagnostics, Hayward, CA, USA) [E6, E7]. Sections were incubated with endogenous enzyme block,

boiled in pretreatment buffer, and treated with protease prior to target probe hybridization (CCL11, CCL24). The target RNA was then amplified using a series of amplification solutions and visualised with coloured chromogen [E6, E7].

Quantitative immunohistochemistry and computerised image analysis

Large IHC- and ISH-stained sections were digitised using a ScanScope slide scanner (Aperio Technologies, Vista, CA, USA). The high-resolution >300 MB images were subjected to computerised image analysis. Briefly, the immunoreactivity and detection chromogens were automatically detected and were quantified automatically by colour segmentation, and the total amount of marker-positive pixels were related and normalised to the tissue background pixels in the analysed region (Visiomorph™ v 4.6.3.857, Visiopharm®, Hoersholm, Denmark) [E8]. For the main study and bulk quantification of the eosinophil, basophil, and GATA3 triple-stained sections, locked threshold values and colour segmentation algorithms were set to automatically detect and quantify each chromogen without any overlap (brown DAB chromogen for GATA3, Vina Green™ for eosinophils/EG2, and permanent red substrate-chromogen for basophils/BB1).

In order to analyse distinct tissue regions, the epithelium, airway wall, pulmonary vessels, alveolar parenchyma, and lymphoid, aggregates were delineated on blinded digitalised sections by manual cursor tracing. For each participant in the main study, several large sections containing bronchioles, pulmonary vessels, and alveolar parenchyma were analysed from 2–3 separate peripheral lung regions. In total, 373 small airways (bronchioles) were analysed, derived from the control (n=93), GOLD I–III (n=167), and GOLD IV COPD (n=123) groups. For all airways, the total airway wall, the epithelial lining, and entire subepithelial tissue were analysed. The cell density in each compartment was calculated as

the number of cells/assessed tissue area. A similar approach was used for peripheral tissues. Peripheral lung tissue was defined as the more distal tissue that remains after removing any large airways or large pulmonary vessels during the gross dissections (i.e., large sections of mainly alveolar parenchyma but with occasional smaller blood vessels, small airways, lymphoid aggregates, and small fibrotic lesions). At least three separated lung regions (and three bronchial blocks) were assessed from each patient in the GOLD IV category, whereas at least two regions were assessed in the other patient groups. Alveolar parenchyma was defined as the alveolar tissue only (e.g., after small airways and larger vessels have been excluded from the analysis by manual cursor tracing), whereas lymphoid tissue–associated cells referred to cells in the tissue directly surrounding ectopic lymphoid tissue. Importantly, for all compartments, the analysis of cell density was expressed as cells/area of proper tissue (after any air spaces, vessel lumen, or larger tissue cracks have been segmented and excluded by a tissue detection algorithm, including removal of the white "air" background).

Eosinophil and basophil clustering

Semi-manual quantification of clusters

Initial manual inspection of the eosinophil, basophil, and GATA3-stained sections revealed several cases of marked patchiness and cell clustering (exemplified in Figure E3). To get a quantitative estimate of such eosinophil and/or basophil clusters, they were counted manually on blinded high-resolution digital image files of the EG2, BB1, and GATA3 triple-stained sections. For this analysis, a cluster was defined as presence of multiple immuno-stained cells (eosinophils or basophils) within a defined circle (100 μm in diameter) with a clear absence of cells in the neighbourhood outside the circle. Such eosinophil and/or basophil clusters were also evaluated for their content of any GATA3-positive cells and expressed as average of clusters/cm lung tissue.

Point pattern analysis to confirm spatial eosinophil clustering

The manual quantification of cell eosinophil clusters was also complemented with spatial statistics and point pattern analysis. Briefly, X,Y coordinates were generated from computer-segmented, immune-stained eosinophils (CC, Medetect, Lund, Sweden) and were used for point pattern analysis of degree of clustering. The statistical models selected for this (nearest neighbour distance analysis and Ripley's K point pattern analysis) require a predominantly convex domain of background tissue and sufficient eosinophils within the selected region of interest, limiting the analysis to six cases from the GOLD IV COPD group. After a Donnelly's correction for edge effect [E9], nearest neighbour distance analysis revealed a highly spatially clustered pattern ($p<0.001$) in the analysed cases.

Spatial analysis of co-clustering of eosinophil and GATA3$^+$ cells

A neighbourhood analysis principle was used to analyse the density of GATA3$^+$ cells inside and outside eosinophil microenvironments in numerous double-stained, eosinophil-rich sections. Each EG2-immunoreactive eosinophil was identified by computerised image analysis, as previously described. Next, a virtual circle with a fixed radius was created around each eosinophil (Cell Community Viewer, CCV 1.22, Medetect, Lund, Sweden) (Figure E1). Three radii were applied (10 μm, 20 μm, and 40 μm), corresponding to three defined sizes of eosinophil neighbourhoods. Using information about GATA3-segmented marker objects, quantitative data of GATA3 density inside and outside eosinophil neighbourhoods were automatically generated and used to calculate the density of GATA3 within and without eosinophil microenvironments, expressed as the ratio: $GATA3^{\text{Eos neighbourhood}}$ / $GATA3^{\text{Non-eos neighbourhood}}$. For each analysed image, the mean density was calculated as total GATA3 immunoreactivity area/total eosinophil neighbourhood area (or total noneosinophil area in the case of $GATA3^{\text{Non-eos}}$).The hypothesis that the eosinophil tends to occur in spatial regions

with a particularly high density of GATA3+ cells was also tested using Monte Carlo simulations, as previously described for eosinophil and ILC2 co-distribution [E5]. Briefly, using the MOSAIC Interaction Analysis Plugin for Fuji/ImajeJ [E10), a circular neighbourhood was defined around each of the eosinophil locations (x,y coordinate). The number of GATA3 in each of these neighbourhoods was counted and added to produce a count for the entire group of cells. The distribution of the simulation round GATA3 counts under the null hypothesis of random placement was determined by 10^4 simulation rounds of eosinophil locations randomly placed within the study area and calculating the group GATA3 count measure for each simulated group. A simple proportional edge correction was applied to neighbourhood counts when part of the circular neighbourhood fell outside the study area.

Analysing the sections with patchy eosinophilia, the null hypothesis could be rejected with a significance level of $p<0.001$, showing that the density of GATA3 cells around the eosinophil locations is indeed significantly higher than would be expected by chance.

Appendix 2. Results: supplemental images

In total, 75 patients with chronic obstructive pulmonary disease (COPD) and controls were included in the study. For the main study, which included patients with COPD and controls (N=45), surgical tissues were collected at Skåne University Hospital in Lund, Sweden, and processed for histologic analysis, as previously described [E1, E2]. Patient groups and clinical characteristics of those in the main study are presented in Table E2.

Bronchial biopsies and tissues samples from 30 separate patients (n=13) and controls (n=17) were used to collect appropriate messenger ribonucleic acid (mRNA)-preserved tissues for *in-situ* hybridisation (ISH). These patient groups and clinical characteristics are presented in Table E2.

The following supplemental images are presented to support the Results section in the main manuscript:

- Micrographs illustrating the principle of automatic detection of eosinophil neighbourhoods in order to reveal a spatial link between $GATA3^{+}$ cells and eosinophil microenvironments (Figure E1)
- Density of eosinophils and basophils in the bronchial biopsy cohort (Figure E2)
- Greater magnification of a spatially distinct eosinophil and GATA3-rich microenvironment (Figure E3)
- Co-emergence of CCL-24 (eotaxin 2) and eosinophil in influenza A–challenged mouse lungs (Figure E4)

Table E1. Antibodies for Immunohistochemical Analysis

Antigen	Clone	Host/ Isotype	Supplier	Antigen Retrieval	Dilution	Against	Secondary Antibody, EnVision™ Detection System Kit, Dako
ECP	EG2	Mouse/ $mIgG_1$	Diagnostics Development	Low pH[#] PT	1:500	Eosinophils	Polymer anti-mouse HRP, K8010
BB1	BB1	Mouse/ $mIgG_2a$	Provided by Dr. Andrew Walls, Southampton, UK	Low pH[#] PT	1:50	Basophils	Polymer anti-mouse AP, K5361
GATA3	L50-823	Mouse/ $mIgG_1\kappa$	BD Biosciences BD Pharmingen™	Low pH[#] PT	1:2,000	Transcription factors	Polymer anti-mouse HRP, K5361
CD68	PG-M1	Mouse/ $mIgG_3\kappa$	Dako	Low pH PT	1:200	Monocytes and macrophages	Polymer anti-mouse , HRP K5361
CD31	C8/ 1448	Mouse/ Ig	Dako	Low pH PT	1 :100	Endothelial cells	Polymer anti-mouse HRP, K5361
CD8	JC70A	Mouse	Dako	Low pH PT	1 :640	Cytotoxic T cells	Polymer anti-mouse HRP, K5361
CD 25	4C9	Mouse/ $mIgG_2b$	Novocastra NCL/Leica	Low pH PT	1:50	IL-2 receptors	Polymer anti-mouse HRP, K5361
GATA3	L50-823	Mouse/ $mIgG_1\kappa$	BD Biosciences	Low pH PT	1:1,000	Transcription factors	Polymer anti-mouse HRP, K5361
CD4	4B12	Mouse/ $mIgG_1$	Novocastra NCL/Leica	High pH[¶]	1:50	T-helper cells	Polymer anti-mouse HRP, K5361
GATA3	L50-823	Mouse/ $mIgG_1$	BD Biosciences	High pH[¶]	1:2,000	Transcription factors	Polymer anti-mouse HRP, K5361

[#]EnVision™ FLEX Target Retrieval Solution, Low pH 6.1, K8005, Dako.
[¶]EnVision™ FLEX Target Retrieval Solution, High pH 9, K8010, Dako.

Table E2. Study Participant Demographics (Bronchoscopy Study)

Parameters	**Former Smokers**	**COPD (GOLD I–III[#])**	**Never-smokers**
Patients	9	13	8
Age, years	67 (64–71)	66 (45–74)	23 (21–39)
Sex, male/female	6/3	9/4	3/5
Body mass index, kg/m^2	27.14 (13.50–33.20)	26.03 (18.65–30.37)	23.01 (19.38–27.10)
Smoking history, pack-years	30 (17–48)	36 (14–159)	NA
$FEV_{1,}$ L (after β_2-agonist)	3.2 (1.9–3.7)	1.6 (0.7–2.6)	3.6 (2.3–5.3)
FEV_1, % predicted (after β_2-agonist)	91.9 (88.1–132.3)	52.0 (28.3–82.1)	98.05 (72.10–116.40)

COPD, chronic obstructive pulmonary disease; FEV_1, forced expiratory volume in 1 second; GOLD, Global Initiative for Chronic Obstructive Lung Disease; NA, not applicable. Values are median (range) or n.

[#]The COPD GOLD I–III cohort composition is: GOLD I (n=1), GOLD II (n=8), and GOLD III (n=4).

Appendix 3. Figures

Figure E1. Micrographs illustrating the principle of automatic detection of eosinophil neighbourhoods in order to reveal a spatial link between GATA3^{+} cells and eosinophil microenvironments. (a and b) Vina green chromogen-stained eosinophils have been detected with colour segmentation and automatically labelled with a dark blue pseudo colour. The turquoise areas represent the automatically generated virtual circular "eosinophil neighbourhood" areas that are created around each eosinophil object. (c and d) Low-power overview images of bronchioles in COPD lungs where 40-µm virtual circular eosinophil neighbourhoods are labelled yellow. Computer-segmented eosinophils are labelled blue and DAB-positive GATA3 cells green. The mucosal subepithelial lamina propria tissue is labelled dark grey.

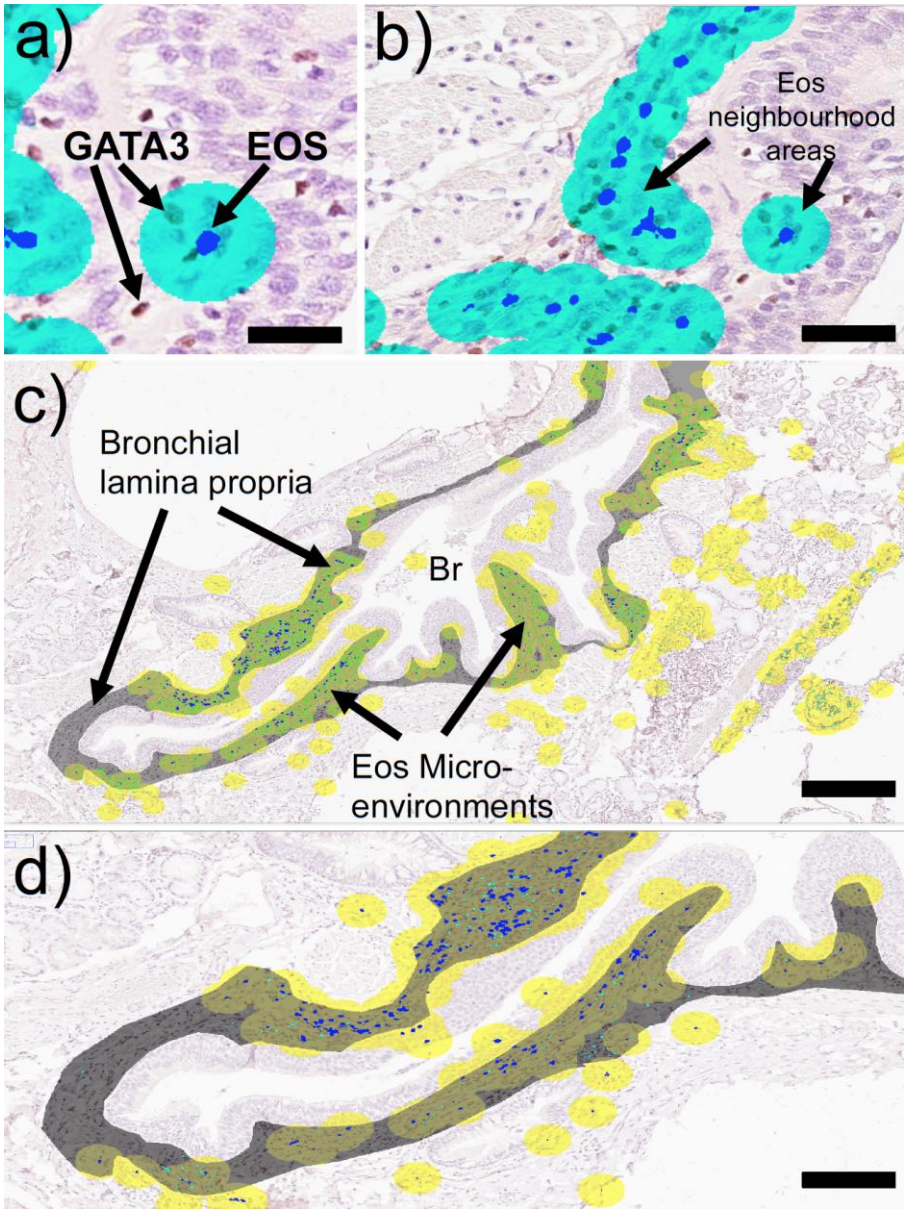

Scale bars: a=25 µm, b=40 µm, c=80 µm, d=65 µm.
COPD, chronic obstructive pulmonary disease; DAB, diaminobenzidine.

Figure E2. Panels a and b show eosinophil and basophil numbers in the separate bronchial biopsies, collected from the bronchoscopy study (from GOLD I–III patients with COPD). Dots represent mean patient values and horizontal dashes represent group mean values. Panels in C show the tissue density of eosinophils, basophils, and GATA3 in bronchioles (small airways) and bronchi in very severe COPD.

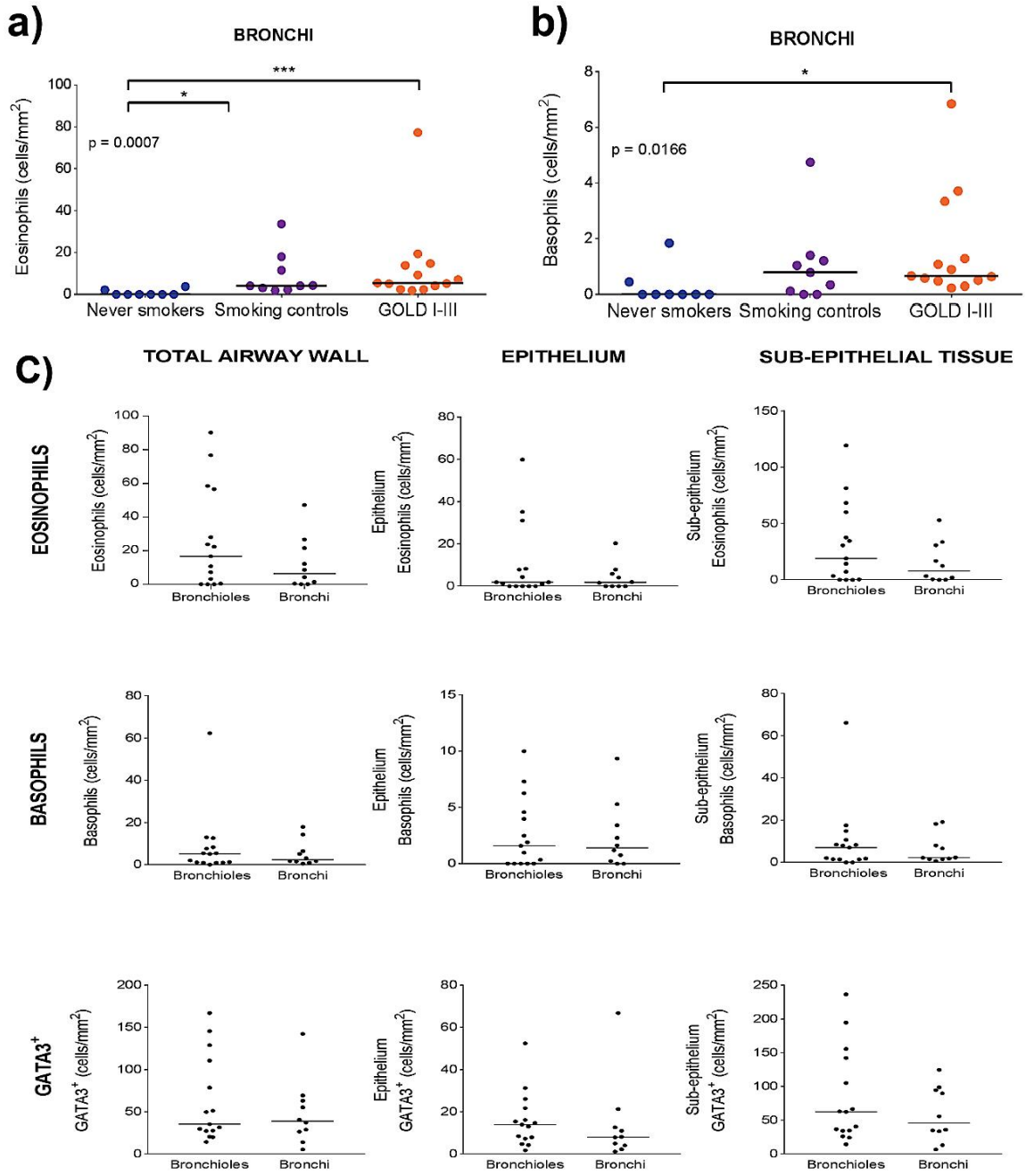

Asterisks denote degrees of statistical significance between groups: *p<0.05; ***p<0.001. P-values quoted in the figure represent overall statistical difference between patients with COPD and controls, as determined by a non-parametric Kruskal-Wallis one-way ANOVA with Dunn's multiple comparison *post-hoc* test (mean rank of each subgroup is compared with every other subgroup). No statistical differences were found between bronchi and bronchioles in C.

COPD, chronic obstructive pulmonary disease; GOLD, Global Initiative for Chronic Obstructive Lung Disease.

Figure E3. (a) Multi-stained tissue section of a small COPD bronchi that exemplifies a spatially distinct eosinophil and GATA3-rich foci, labelled here as a Th_2-skewed pocket. Eosinophils were identified by EG2 immunoreactivity and pseudo coloured red whereas $GATA3^+$ cells are marked bright green. (b) Greater magnification of the same section and Th_2 pocket, where cell nuclei also have been pseudo coloured (blue).

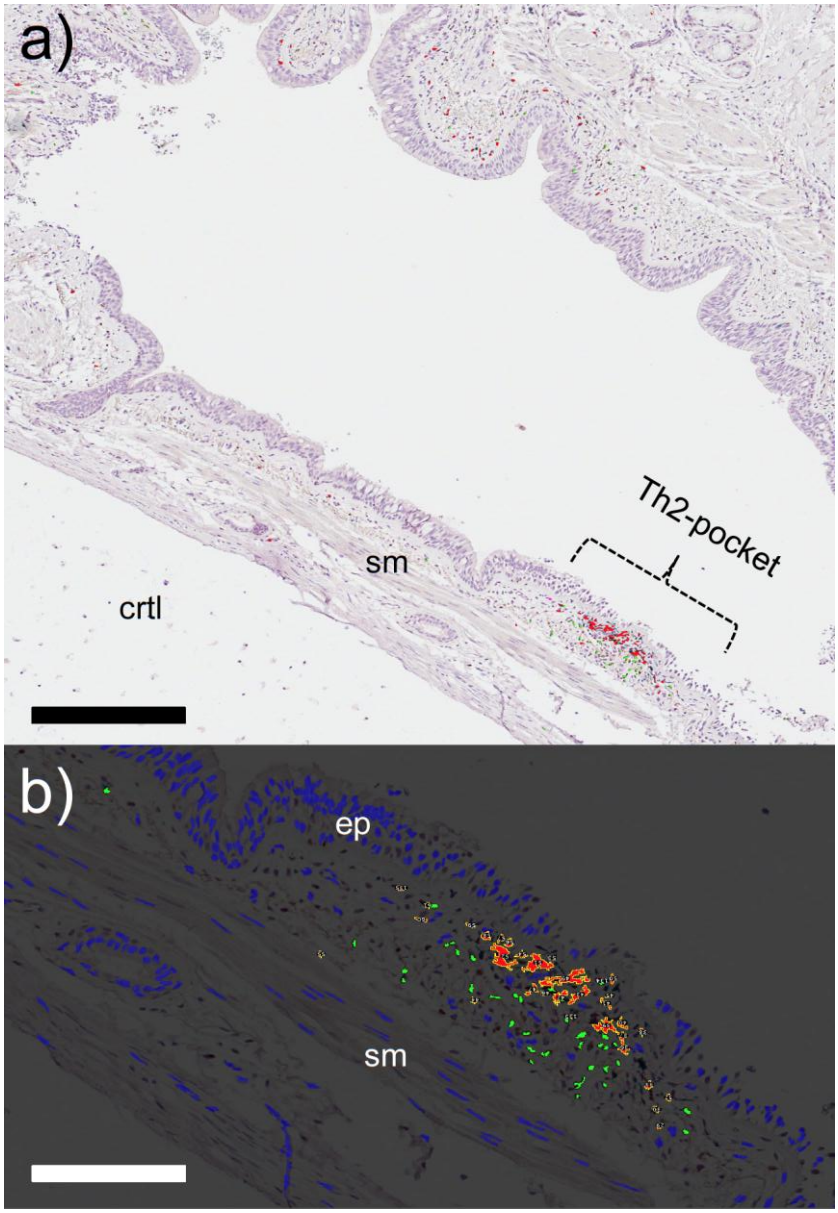

Scale bars: a=350 µm, b=150 µm.
COPD, chronic obstructive pulmonary disease; ctrl, bronchial cartilage; ep, bronchial epithelium; sm, smooth muscle.

Figure E4. Spatial correlation between localized CCL11 (eotaxin 1) and CCL-24 (eotaxin 2) and eosinophils in localized influenza A–infected mouse lung areas. Examples of percentages of tissue area positive for ISH-detected CCL11 (a) and CCL24 (b) mRNA in virus-low (grey) and virus-high (black) lung regions in representative individual mice. (c) Bright field image of CCL-24 mRNA, as detected by *in-situ* hybridisation and brown DAB detection chromogen. (d) The same lung area stained for eosinophils (green fluorescence; DAPI was used for blue cell nuclei detection).

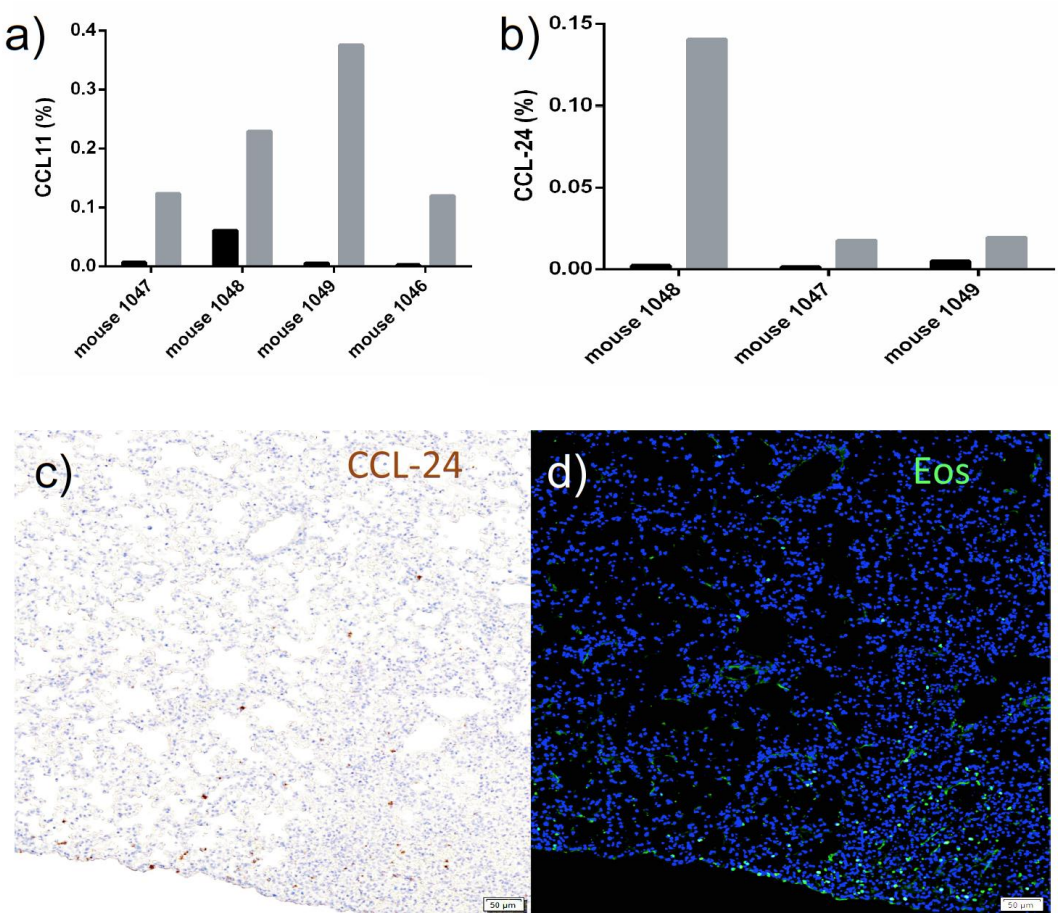

Scale bars: 50 µm.
DAB, diaminobenzidine; DAPI, 4',6-diamidino-2-phenylindole; ISH, in situ hybridisation; mRNA, messenger ribonucleic acid.

Appendix 4. References

E1. Roos AB, Sanden C, Mori M, et al. IL-17A is elevated in end-stage chronic obstructive pulmonary disease and contributes to cigarette smoke-induced lymphoid neogenesis. *Am J Respir Crit Care Med* 2015; 191: 1232–1241.

E2. Mori M, Andersson CK, Svedberg KA, et al. Appearance of remodelled and dendritic cell-rich alveolar-lymphoid interfaces provides a structural basis for increased alveolar antigen uptake in chronic obstructive pulmonary disease. *Thorax* 2013; 68: 521–531.

E3. Das J, Chen CH, Yang L, et al. A critical role for NF-kappa B in GATA3 expression and TH2 differentiation in allergic airway inflammation. *Nat Immunol* 2001; 2: 45–50.

E4. Nakayama T, Hirahara K, Onodera A, et al. Th2 Cells in Health and Disease. *Annu Rev Immunol* 2016; 35: 53–84.

E5. Bal SM, Bernink JH, Nagasawa M, et al. IL-1beta, IL-4 and IL-12 control the fate of group 2 innate lymphoid cells in human airway inflammation in the lungs. *Nat Immunol* 2016; 17: 636–645.

E6. Wang F, Flanagan J, Su N, et al. RNAscope: a novel in situ RNA analysis platform for formalin-fixed, paraffin-embedded tissues. *J Mol Diagn* 2012;14:22–29.

E7. Silver JS, Kearley J, Copenhaver AM, et al. Inflammatory triggers associated with exacerbations of COPD orchestrate plasticity of group 2 innate lymphoid cells in the lungs. *Nat Immunol* 2016;17: 626–635.

E8. Bergqvist A, Andersson CK, et al. Alveolar T-helper type-2 immunity in atopic asthma is associated with poor clinical control. *Clin Sci (Lond)* 2015;128:47–56.

E9. Hammer Ø. New methods for the statistical analysis of point pattern alignments. *Comput Geosci* 2009; 35: 659–666

E10. Shivanandan A, Radenovic A, Sbalzarini IF. MosaicIA: an ImageJ/Fiji plugin for spatial pattern and interaction analysis. *BMC Bioinformatics* 2013;14:349.